



## Original Paper

# Characteristics, main controlling factors and densification mechanisms of unconventional tight reservoirs in Triassic Yanchang Formation in southern Ordos Basin, China



Yi-Quan Ma <sup>a, b</sup>, Chen Zhang <sup>a, b, \*</sup>, Yong-Chao Lu <sup>c</sup>, Xiang-Ye Kong <sup>a, \*\*,</sup>, Ying Guo <sup>a, d</sup>,  
Yi-Xin Dong <sup>a</sup>, Lin Chen <sup>e</sup>, Rong Qi <sup>f</sup>, Feng-Cun Xing <sup>a, b, \*\*\*</sup>

<sup>a</sup> State Key Laboratory of Oil and Gas Reservoir Geology and Exploitation & Institute of Sedimentary Geology, Chengdu University of Technology, Chengdu, 610059, Sichuan, China

<sup>b</sup> Key Laboratory of Deep-time Geography and Environment Reconstruction and Applications of Ministry of Natural Resources, Chengdu University of Technology, Chengdu, 610059, Sichuan, China

<sup>c</sup> College of Earth Resources, China University of Geosciences (Wuhan), Wuhan, 430074, Hubei, China

<sup>d</sup> College of Management Science, Chengdu University of Technology, Chengdu, 610059, Sichuan, China

<sup>e</sup> Wuhan Center of China Geological Survey, Wuhan, 430205, Hubei, China

<sup>f</sup> Research Institute of Petroleum Exploration and Development, North China Oil and Gas Company, Sinopec, Zhengzhou, 450006, Henan, China

## ARTICLE INFO

## Article history:

Received 8 January 2024

Received in revised form

1 August 2024

Accepted 24 September 2024

Available online 26 September 2024

Edited by Jie Hao

## Keywords:

Yanchang formation

Tight reservoirs

Densification process

Ordos basin

Reservoir evaluation

## ABSTRACT

The key factors controlling the densification of unconventional reservoirs (e.g., tight oil and gas reservoirs) remain poorly understood and directly affect the distribution of exploitable resources. Here, systematically explored reservoir characteristics, depositional microfacies, and the main factors controlling densification of the tight oil reservoir in the Chang 8 Member (Yanchang Formation, Middle Triassic) in the southern Ordos Basin by thin section analysis, scanning electron microscopy, physical property measurement, X-ray diffraction, and mercury injection. Our results confirm the Chang 8 reservoir as an extremely low permeability tight sandstone reservoir mainly comprising lithic feldspathic sandstone with various primary and secondary pores and fine pore channels. The highest quality reservoir is mainly restricted to the middle and lower parts of subaqueous distributary channel microfacies. Dissolution partly contributed to reservoir formation, but the persistence of early, non-compressed storage space was more important. The compression of plastic rock debris removed a significant amount of porosity, and calcite, kaolinite, and siliceous minerals both fill pores, whereas chlorite cladding of particles protects the pore space. We identified three densification mechanisms: the persistent densification of highly plastic rock debris during burial, calcite cementation and pore filling, and feldspar dissolution and subsequent kaolinite precipitation and siliceous cementation. After their compaction, the Chang 8 Member reservoirs were charged with hydrocarbons. We applied clustering analysis to eight reservoir characteristics (porosity, permeability, median pore-throat radius, maximum pore-throat radius, median capillary pressure, pore discharge pressure, chlorite content, kaolinite content) to quantitatively classify the Chang 8 reservoir into three categories. Type-I reservoirs have the best conditions for hosting tight oil reservoirs, with ~12% porosity, permeabilities of  $\sim 0.2 \times 10^{-3} \mu\text{m}^2$ , trial oil production rates of  $>5 \text{ m}^3/\text{d}$ , and, indeed, occur in subaqueous distributary channel microfacies. Type-II reservoirs ~10% porosity, permeabilities of  $\sim 0.1 \times 10^{-3} \mu\text{m}^2$ , and trial oil production rates of  $1\text{--}5 \text{ m}^3/\text{d}$ . Type-III reservoirs have ~5% porosity, permeabilities of  $\sim 0.05 \times 10^{-3} \mu\text{m}^2$ , and trial oil production rates  $<1 \text{ m}^3/\text{d}$ . These results provide

\* Corresponding author. State Key Laboratory of Oil and Gas Reservoir Geology and Exploitation & Institute of Sedimentary Geology, Chengdu University of Technology, Chengdu, 610059, Sichuan, China.

\*\* Corresponding author.

\*\*\* Corresponding author. State Key Laboratory of Oil and Gas Reservoir Geology and Exploitation & Institute of Sedimentary Geology, Chengdu University of Technology, Chengdu, 610059, Sichuan, China.

E-mail addresses: [zhangchen2022@cdut.edu.cn](mailto:zhangchen2022@cdut.edu.cn) (C. Zhang), [kongxiangyecup@163.com](mailto:kongxiangyecup@163.com) (X.-Y. Kong), [xingfengcun@163.com](mailto:xingfengcun@163.com) (F.-C. Xing).

an important basis for predicting the distribution of exploitable zones in the Chang 8 Member and other adjacent tight reservoirs.

© 2024 The Authors. Publishing services by Elsevier B.V. on behalf of KeAi Communications Co. Ltd. This is an open access article under the CC BY-NC-ND license (<http://creativecommons.org/licenses/by-nc-nd/4.0/>).

## 1. Introduction

Extremely low permeability tight sandstone reservoirs have increased global oil and gas production, and their utility has promoted unconventional petroleum development, which has become a global concern (Ameen et al., 2012; Yang et al., 2017a; Debenham et al., 2019; Gao et al., 2020; Li et al., 2021; Cui and Radwan, 2022; Xie et al., 2022). Tight sandstones in China host abundant oil and gas resources, including nearly  $14 \times 10^8$  t of recoverable tight oil and nearly  $13 \times 10^{12}$  m<sup>3</sup> of recoverable tight gas (Jia et al., 2012). The Zhenjing area in the southern Ordos Basin is important to exploration efforts seeking oil in extremely low permeability tight sandstones. Recently, several development blocks have been established in this area, including the Honghe oil field (Jia et al., 2016; Ma et al., 2020), which has high potential for tight oil resources. One of the most important oil-producing reservoirs in this area is the Middle Triassic Chang 8 Member (Yanchang Formation), which comprises a sequence of extremely low permeability and strongly spatially heterogeneous tight sandstone reservoirs.

The Chang 8 Member reservoir is typical of tight sandstone reservoirs in the Zhenjing area. Its complex and diverse sedimentary environments provide ideal conditions for studying reservoir densification mechanisms. The Chang 8 Member reservoir is considered to have high resource potential and is a key target for the development of the Honghe oilfield (Zhang et al., 2012; Liang and Guo, 2017; Wang et al., 2017; Ma et al., 2020). Prior works on the Chang 8 Member reservoir in the Zhenjing area have focused on sequence stratigraphy and sedimentary facies (Chen et al., 2015), reservoir characteristics and diagenesis (Ding et al., 2011; Zhang et al., 2012; Liang and Guo, 2017; Wang et al., 2017, 2018), the relationship between reservoir densification and oil accumulation (Zhou et al., 2016; Ma et al., 2020), reservoir classification and evaluation (Lin et al., 2017), and microfracture characteristics and development (Lv et al., 2020). Of those, some studies have indicated that high-quality reservoirs are mainly developed in subaqueous distributary channels (Zhang et al., 2012; Lin et al., 2017; Wang et al., 2017), whereas Ding et al. (2011) suggested that high-quality reservoirs are mainly developed in sheet sand microfacies atop the river-mouth bar. Based on microfacies and pore structures, other studies concluded that the river-mouth bar itself, like the subaqueous distributary channels, can also host high-quality reservoirs (Zhou et al., 2016; Wang et al., 2021).

In addition to these discrepancies regarding where tight reservoirs have developed in the Chang 8 Member, how they developed also remains disputed. Wang et al. (2017, 2021) suggested that sedimentary microfacies are the primary factor controlling the physical properties of the reservoirs and thus represent the material basis for the development of high-quality reservoirs. In contrast, several studies found that diagenesis has a greater impact on tight reservoir quality and that compaction is the main factor controlling reservoir quality (Liang and Guo, 2017; Wang et al., 2018). Both Li et al. (2011) and Lin et al. (2017) attempted to quantitatively classify and evaluate the quality of the Chang 8 Member reservoir in the study area using multivariate statistical methods; however, they chose contrasting parameters for their

reservoir evaluations and obtained quite different results.

To summarize, prior studies have not reached a consensus on which sedimentary microfacies are conducive to the development of high-quality reservoirs, which main factors control the development of high-quality reservoirs, which parameters should be used to evaluate reservoirs and analytical results, or which key factors control the densification of tight sandstones. All these discrepancies have hindered exploration and development of the Chang 8 Member reservoir in this area. Although previous studies have revealed some densification mechanisms, our understanding of the interactions and comprehensive effects of different densification mechanisms within specific geological environments remains insufficient. In particular, few systematic, multi-parameter comprehensive studies have evaluated the impacts of different densification mechanisms on reservoir quality and hydrocarbon accumulation. Furthermore, studies classifying and evaluating tight sandstone reservoirs are mostly limited to single-parameter analyses that cannot fully capture the comprehensive impacts of multiple parameters, thus limiting their accuracy and scientific validity.

This study aims to systematically analyze and evaluate the Chang 8 Member tight sandstone reservoirs in the Zhenjing area of the Triassic Yanchang Formation, with a focus on densification mechanisms and their impacts on reservoir quality. We combine results from previous studies with a systematic analysis by integrating multiple techniques for studying tight sandstone reservoirs, including thin section observations, physical property testing, mineralogical analysis by X-ray diffraction (XRD), scanning electron microscopy, mercury intrusion analysis, and quantitative reservoir evaluation by cluster analysis (Yang et al., 2017a; Wang et al., 2018; Lv et al., 2020; Cui and Radwan, 2022; Xie et al., 2022). Our results improve the current understanding of the development and characteristics of extremely low permeability tight sandstone reservoirs, specifically the mechanism by which high-quality reservoirs form in the Zhenjing area. Our results should therefore provide an improved scientific basis for oil and gas exploration and the development of tight reservoirs.

## 2. Geological background

The Ordos Basin is a large cratonic basin covering an area of about  $32 \times 10^4$  km<sup>2</sup> (Yang et al., 2005). During the Triassic, the basin was in a temperate to subtropical climate zone in the western part of the North China Plate at about 30° N (Fig. 1(a)) (Ji et al., 2010). The Ordos Basin includes six secondary structural units: (1) the Yimeng uplift in the north, (2) the fault-folded belt and (3) Tianhuan Depression in the west, (4) the central Yishan slope, (5) the Weibei uplift in the south, and (6) the Jinxi flexure fold belt in the east (Fig. 1(b)) (Yang et al., 2005; Li et al., 2014; Dou et al., 2017). Tectonically, the Ordos Basin is a north-south rectangular basin with a broad, shallow eastern slope and a narrow, steep western slope. Fault folds are developed in the basin margins, whereas the internal tectonics of the basin are relatively simple and the strata slope gently (e.g., Yang et al., 2005; Ritts et al., 2009). During the deposition of the Yanchang Formation, the Ordos Basin was

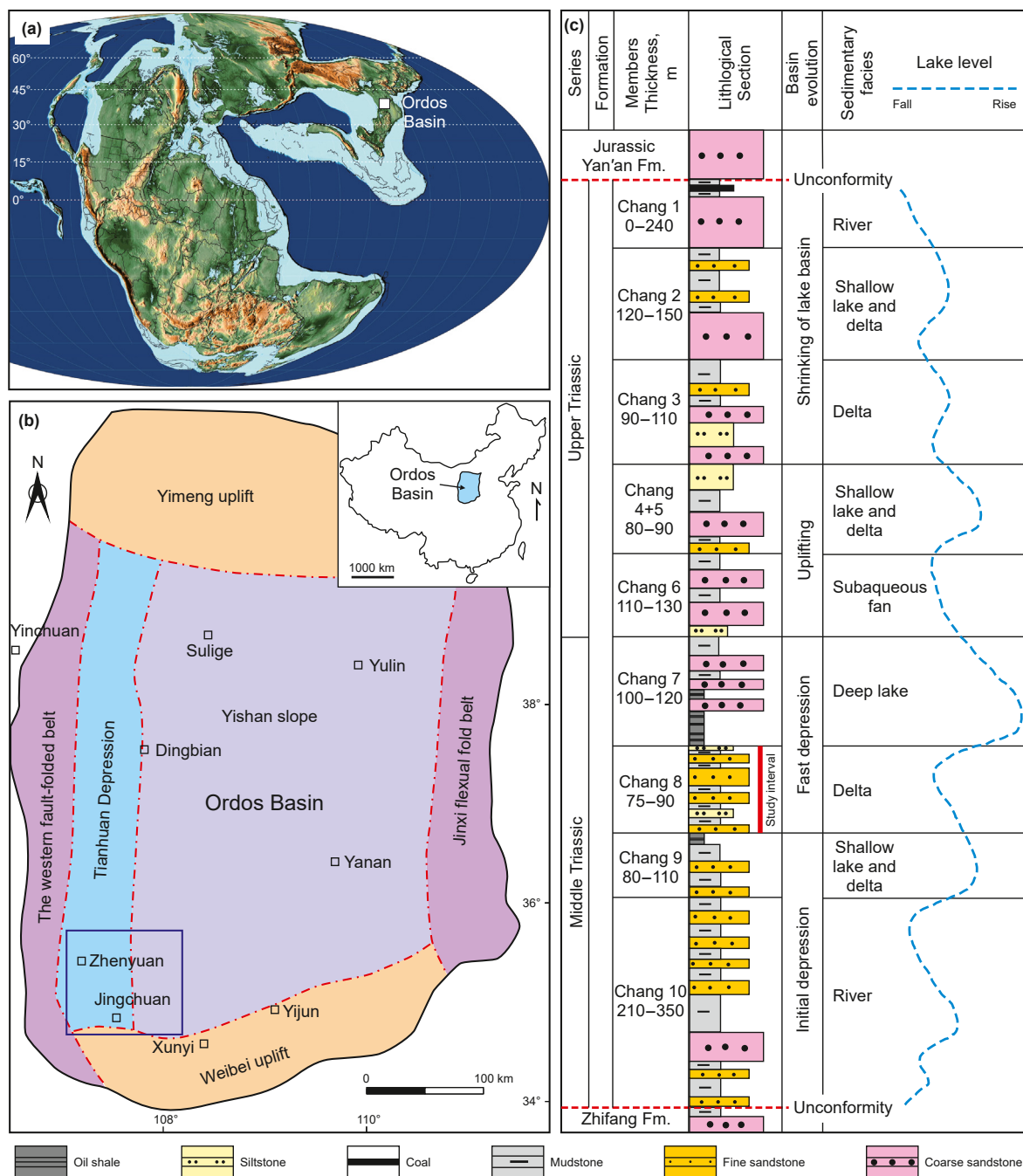


**Fig. 1.** (a) Middle Triassic paleogeographic reconstruction and the general location of the Ordos Basin at that time (Scotese, 2014). (b) Present-day location of the Ordos Basin in China, tectonic subunits of the Ordos Basin, and the location of the Zhenjing area (dark blue square). (c) Stratigraphic column and inferred lake-level fluctuations of the Yanchang Formation in the study area. Modified from Yang et al. (2017b) and Jin et al. (2021).

shallow-sloped and received gentle deposition in a stable cratonic setting, mainly developing river–lacustrine delta facies (Fig. 1(c)) (e.g., Zou et al., 2010; Yang and Deng, 2013; Deng et al., 2018).

The Yanchang Formation is divided into ten oil-bearing formations: from top to bottom, they are the Chang 1 to Chang 10 Members (Fig. 1(c)) (Duan et al., 2008; Yang and Deng, 2013; Qiu et al., 2014; Deng et al., 2018). The Chang 8 Member, which is in the lower part of the Yanchang Formation, has been suggested to be deposited during late Anisian of Middle Triassic (e.g., Liu et al., 2023). The Chang 8 Member is conformably overlain by the Chang 7 Member, the ‘Zhangjiatan shale’, which mainly developed

in a deep lake setting (Fig. 1(c)). In the Zhenjing area (~2500 km<sup>2</sup> in the southern Tianhuan Depression), the Chang 8 Member is mainly developed in a prograde braided-river delta sedimentary system that was dominated by a delta-front environment (e.g., Chen et al., 2015). Lithologically, the Chang 8 Member mainly comprises fine gray sandstone and siltstone intermixed with dark mudstone. Various sedimentary structures such as cross-bedding and deformation structures are developed, and oil spots, oil dips, and oil traces are commonly observed. The Chang 8 Member in the Zhenjing area is one of the most productive beds in the Ordos Basin (Fig. 1(b) and (c)).

### 3. Materials and methods

#### 3.1. Thin section observations

We selected a total of 221 samples of Chang 8 Member sandstone from 14 wells in the study area for thin section observation. The samples were cut into small pieces measuring 25 mm × 25 mm × 5 mm, and the 25 mm × 25 mm surface was polished. The polished surface was glued to a glass slide using resin, compacted, dried, and fixed on a cutting machine. The samples were then thinned to 0.5 mm thickness. The 0.5-mm-thick samples were then fixed on a polishing thickness controller for further thinning and polishing to 0.03 mm thickness. Samples with regular areas were stained with blue epoxy and covered with a cover slip. Thin section observations were performed using a ZEISS Axioskop 40 polarizing microscope at room temperature (23 °C).

#### 3.2. Porosity and permeability and mineral compositions

The porosity and permeability data of the 889 core samples from 23 wells used in this study were analyzed using the porosity and permeability measurement system, provided by Sinopec North China Oil and Gas Company. Calcite content and different clay mineral contents (e.g., chlorite and kaolinite contents) were analyzed using X-ray diffraction (XRD) and their weight percentages were obtained by computer analysis of the diffractograms.

#### 3.3. Mercury intrusion tests

Constant-pressure mercury testing was conducted on 15 representative reservoir samples in the study area using a 9505 Rock Pore Structure Analyzer (mercury porosimeter). Prior to testing, the samples were dried in an oven at <90 °C for at least 4 h. The maximum mercury inlet pressure of the instrument is 32.1 MPa. After installing the expansion joint, low-pressure microcomputer operation and high-pressure microcomputer operation were performed sequentially. Parameters such as capillary pressure, pore throat radius, pore radius, and the pore throat distribution frequency were determined by analyzing data such as mercury saturation during injection and withdrawal, in combination with curve morphology (Hao et al., 2017).

#### 3.4. Parameter selection and cluster analysis

For our reservoir classification, we included petrophysical parameters (porosity, permeability), pore structure parameters (median pore throat radius, maximum pore throat radius, median capillary pressure, pore discharge pressure), and cementation parameters (chlorite and kaolinite contents). These parameters are known to affect reservoir quality and fluid transmission capacity and are widely used in reservoir evaluations (e.g., Bloch et al., 2002; Shou et al., 2005; Lai et al., 2018; Sun et al., 2019). Although certain parameters exhibit positive correlations (e.g., median and maximum pore throat radii, as well as median capillary pressure and pore discharge pressure), their specific values and distribution characteristics in different reservoir types can provide more detailed information about the reservoir microstructure, and thus allow for more accurate classification. Our comprehensive evaluation method ensures the scientific validity and reliability of the classification results. We standardized all parameters to eliminate dimensional or order-of-magnitude differences and ensure balanced weighting in the analysis.

We also used Q-type cluster analysis, which is used to identify correlations among samples as opposed to correlations among variables. This multivariate statistical method is used to

quantitatively classify a sample set by aggregating similar samples step-by-step through a similarity index (Tang et al., 2012; Shi et al., 2019). For the successful implementation of Q-type cluster analysis, the characteristic parameters for reservoir evaluation must first be determined, then similarity statistics (used to measure the degree of similarity between samples) are calculated. Based on the similarity statistics, the highest degrees of similarity are aggregated into a small classification that is gradually broadened to form a classification system from small to large (Fu et al., 2011). The quantitative classification results are visualized in a clustering spectrum diagram, which here provides an objective basis for classifying and evaluating the Chang 8 Member reservoir.

By treating observations of  $m$  variables on  $n$  samples as  $n$  sample points in  $m$ -dimensional space, the distance between any two sample points  $x_a$  and  $x_b$  can be used to measure their similarity as:

$$d_{ab} = \left[ \frac{1}{m} \sum_{i=1}^m (x_{ia} - x_{ib})^2 \right]^{\frac{1}{2}} \quad (1)$$

where  $x_{ia}$  and  $x_{ib}$  denote the  $i$ th characteristic parameters of samples  $a$  and  $b$ , respectively. Dividing both sides by  $m$ , the relative distance  $d_{ab}$  becomes independent of the number of variables; smaller values of  $d_{ab}$  represent higher degrees of similarity between samples.

The sample distance coefficients  $d_{ab}$  calculated according to Eq. (1) form the distance coefficient matrix  $\mathbf{D}$ :

$$\mathbf{D} = \begin{bmatrix} d_{11} & d_{12} & \cdots & d_{1m} \\ d_{21} & d_{22} & \cdots & d_{2m} \\ \vdots & \vdots & \cdots & \vdots \\ d_{n1} & d_{n2} & \cdots & d_{nm} \end{bmatrix} \quad (2)$$

To avoid negative effects that might arise when combining the different units and orders of magnitude of the different variables in the original dataset, we used a common normalization method to pre-process the original data:

$$x_{ia}^* = \frac{x_{ia} - x_{i(\min)}}{x_{i(\max)} - x_{i(\min)}} \quad (3)$$

where  $x_{i(\min)}$  and  $x_{i(\max)}$  are the minimum and maximum values of the  $i$ th characteristic parameter and  $x_{ia}^*$  is the processed datapoint that has a value between 0 and 1.

## 4. Results and discussion

### 4.1. Petrological and physical characteristics

The Chang 8 Member reservoir contains 26%–58% quartz (average 39%), 22%–55% feldspar (average 35%), and 10%–40% rock debris (average 25%) (Fig. 2(a)). Sandstones are dominantly lithic arkose and subordinately feldspathic litharenite. Thin-section observations indicate that quartz is dominated by monocrystalline quartz (Fig. 3), whereas the rock debris is mainly volcanic and metamorphic debris. Matrix contents are mainly 1%–10% (average 2.6%) and cement contents are 0.5%–28% (average 10.7%). Among the sandstones, 52.3% are fine sandstone, 46.8% are medium sandstone, and fewer than 1% are siltstone or coarse sandstone. Grains are mainly sub-angular to sub-rounded and are moderately to well sorted (Fig. 3). Grain contacts are mainly spot-line contacts and subordinately line contacts, and cementation is porous (Fig. 3).

The porosity of the Chang 8 Member reservoir in the Zhenjing

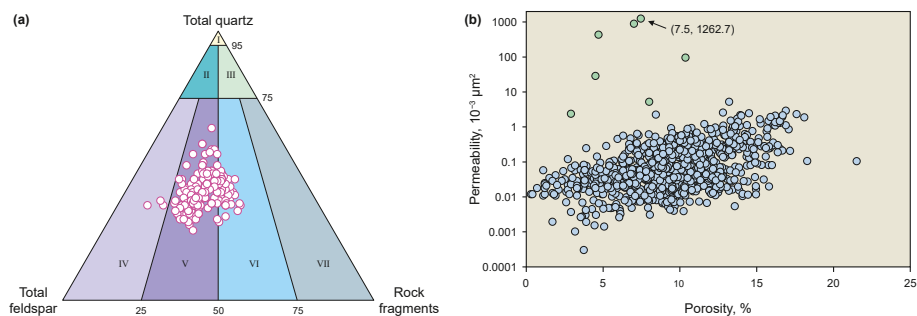


**Fig. 2.** (a) Rock types of the Chang 8 Member tight sandstones in the Zhenjing area. Classification fields after Folk et al. (1970) are (I) quartzarenite, (II) subarkose, (III) sublitharenite, (IV) arkose, (V) lithic arkose, (VI) feldspathic litharenite, and (VII) litharenite. (b) The relationship between the porosity and permeability of the Chang 8 Member in the Zhenjing area. Green symbols indicate samples affected by fractures.

area ranges from 0.3% to 21.5% (average 9.4%) and permeability ranges from  $0.03 \times 10^{-2}$  to  $1262.70 \times 10^{-3} \mu\text{m}^2$  (average  $3.25 \times 10^{-3} \mu\text{m}^2$ ) (Fig. 2(b)). Permeabilities greater than  $3 \times 10^{-3} \mu\text{m}^2$  may be affected by fractures. Pore-throat radii range from 0.02 to 0.53  $\mu\text{m}$  (average 0.14  $\mu\text{m}$ ) and median pore-throat radii from 0.02 to 0.10  $\mu\text{m}$  (average 0.05  $\mu\text{m}$ ). Median capillary pressures range from 3.66 to 62.27 MPa (average 17.92 MPa) and pore discharge pressures from 0.25 to 11.73 MPa (average 3.13 MPa).

#### 4.2. Pore types

Cast thin section observations and quantitative pore-type statistics and distributions reveal five main types of pores in the Chang 8 Member.

- (1) Intergranular dissolved pores formed by the dissolution of primary intergranular micropores and residual primary intergranular pores between feldspar, calcite, rock debris, and other particles (Fig. 3(a)). These pores vary in size and distribution, are irregularly shaped and similar to embayments, and represent about 1.0% of the rock (Fig. 4).
- (2) Intragranular dissolved pores are often developed along cleavage or cracks in calcite, feldspar, and other minerals, and are often developed in combination with intergranular dissolved pores (Fig. 3(b)–(d)). These pores have an uneven distribution and represent about 2.5% of the rock (Fig. 4). These and residual primary intergranular pores dominate hydrocarbon enrichment in the Chang 8 Member.
- (3) Residual primary intergranular pores are the pore space remaining after chlorite rims developed around clastic particles and filled the primary pore space (Fig. 3(a)). These pores represent about 2.0% of the rock (Fig. 4).
- (4) Intergranular micropores occur between chlorite and kaolinite grains. The size of these pores depends on the size of the crystals and the degree of compaction (Fig. 3(e)). These pores account for about 0.5% of the rock (Fig. 4).
- (5) Microfractures are small structural fractures formed by compaction and various tectonic stresses. These fractures are relatively clean and often run through the matrix and plastic debris, significantly increasing the permeability of the Chang 8 Member reservoir. Microfractures are occasionally filled by calcite and siliceous minerals. Like intergranular micropores, microfractures account for about 0.5% of the rock (Fig. 4).

The surface porosity of the Chang 8 Member reservoir mainly varies between 3.0% and 18.0%. Pore types occur in many combinations, including intergranular dissolved pores + residual primary

intergranular pores + intergranular micropores, residual primary intergranular pores + intergranular micropores, intragranular dissolved pores + residual primary intergranular pores, and intergranular dissolved pores + intragranular dissolved pores + intergranular micropores.

#### 4.3. Pore-throat characteristics

In extremely low permeability tight sandstone reservoirs, the shapes, sizes, and distribution of pore throats are important factors affecting reservoir seepage capacity and oil productivity (Liu et al., 2020; Shi et al., 2021). Here, based on our comprehensive analysis of mercury intrusion curves and seepage characteristics, we divided pore throats of the Chang 8 Member into three types, extending the terminology of Zhong et al. (2022) (Fig. 5).

- (1) ‘Microthroats’ are characterized by type-I mercury intrusion curves (Fig. 5(a)) that show a large increase in mercury saturation at low capillary pressures of 0.10–1.00 MPa. Maximum mercury saturation reaches 85–95%, indicating that these pores have relatively wide throats and are highly connected. Displacement pressures for this pore-throat type range from 0.30 to 2.11 MPa (average 0.91 MPa) and the median pressure ranges from 1.18 to 9.65 MPa (average 3.80 MPa). The maximum pore-throat radius ranges from 0.36 to 2.53  $\mu\text{m}$  (average 1.34  $\mu\text{m}$ ), the mean radius from 0.11 to 0.68  $\mu\text{m}$  (average 0.36  $\mu\text{m}$ ), and the median radius from 0.08 to 0.64  $\mu\text{m}$  (average 0.30  $\mu\text{m}$ ). Throat-size sorting coefficients range from 0.06 to 0.56 (average 0.29). The overall porosity generally exceeds 10% (average 11.08%) with permeabilities of  $0.15$ – $2.78 \times 10^{-3} \mu\text{m}^2$  (average  $0.77 \times 10^{-3} \mu\text{m}^2$ ). In terms of oil reservoirs, this pore-throat type is the most exploitable of the three.
- (2) ‘Coarse nanthroats’ are characterized by type-II mercury intrusion curves (Fig. 5(b)), which show less curvature than type-I curves. These mercury intrusion curves increase moderately at capillary pressures around 10 MPa, and maximum mercury saturation reaches 60%–85%. Displacement pressures for this pore-throat type are higher than those for microthroats, averaging 5.04 MPa, and the median pressure ranges from 8.79 to 31.25 MPa (average 14.60 MPa). The maximum pore throat radius is 0.16  $\mu\text{m}$  on average, the mean radius ranges from 0.04 to 0.08  $\mu\text{m}$  (average 0.06  $\mu\text{m}$ ), and the median radius is 0.06  $\mu\text{m}$  on average. The pore-throat radius distribution is unimodal, relatively concentrated, and better sorted (average 0.03) than that for microthroats. The overall porosity is generally less than 10% (average 8.36%) with permeabilities of  $0.16$ – $0.28 \times 10^{-3} \mu\text{m}^2$

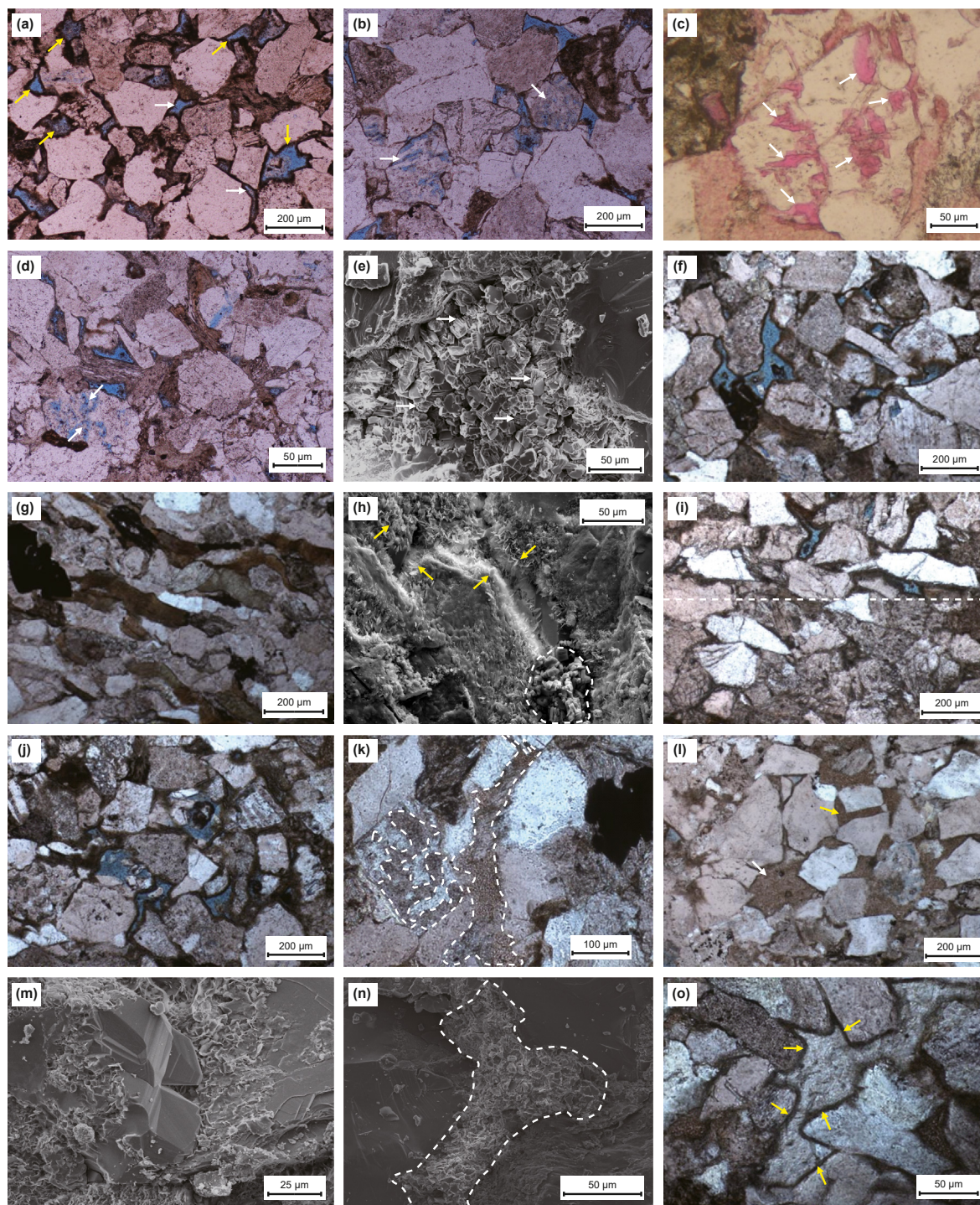


**Fig. 3.** Microscopic features of the Chang 8 Member in the Zhenjing area. **(a)** Intergranular dissolved pores (yellow arrows) and residual primary intergranular pores (white arrows) and **(b)** intragranular dissolved pores (white arrows); well HH87, 2460.94 m depth, plane-polarized light (PPL), blue-cast thin sections. **(c)** Intragranular dissolved pores in feldspar (arrows); well ZJ17, 2260.8 m depth, PPL, Alizarin Red staining, red-cast thin section. **(d)** Intragranular dissolved pores in rock debris (arrows); well HH87, 2486.23 m depth, PPL, blue-cast thin section. **(e)** Intergranular micropores between kaolinite grains (white arrows); well HH113, 2047.28 m depth, SEM image. **(f)** High porosity in a sandstone with little plastic rock debris content; well HH105, 2108 m depth, PPL, blue-cast thin section. **(g)** Low porosity in a sandstone with abundant plastic rock debris; well HH125, 2209.1 m depth, PPL. **(h)** Chlorite rims developed around clastic particles (yellow arrows), and kaolinite filling intergranular micropores (white dashed outline); well HH1057-3, 2237.19 m depth, SEM image. **(i)** Chlorite rims and pores are developed above, but not below, the white dashed line; well HH1057-3, 2234.3 m depth, PPL, blue-cast thin section. **(j)** High porosity in a zone with pervasive chlorite rims; well HH1057-3, 2231.1 m depth, PPL, blue-cast thin section. **(k)** Kaolinite, the dissolution product of feldspar, filling dissolution pores (white dashed outlines); well HH1057-3, 2228.2 m depth, PPL. **(l)** After feldspar dissolves, kaolinite precipitates in situ or near the source, filling both the pores created by feldspar dissolution (white arrow) and nearby primary intergranular pores (yellow arrow); well HH103, 2234.56 m depth, PPL. **(m)** Clay film formed between the edge of a quartz grain and adjacent particles; well HH113-61, 2204.28 m depth, SEM image. **(n)** Kaolinite filling an intergranular micropore; well HH91-101, 1886.77 m depth, SEM image. **(o)** Dissolution primary pores filled by calcite, with chlorite rimming the surfaces of surrounding grains (arrows); well HH1057-3, 2232.13 m depth, PPL.

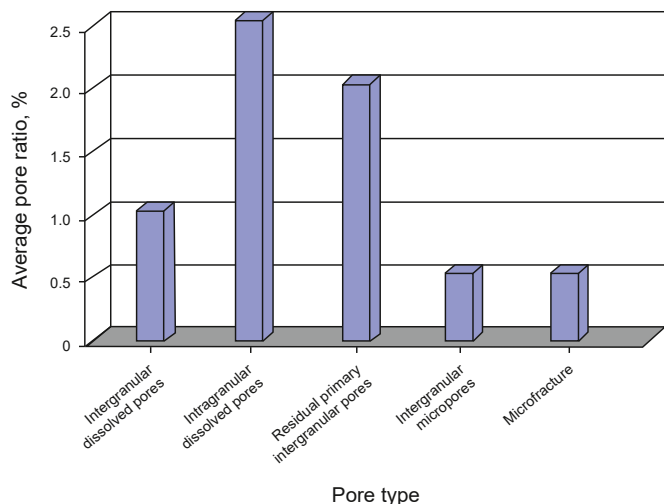


**Fig. 4.** The proportions of different pore types of the Chang 8 Member in the study area, based on 63 samples counted from 3 wells.

(average  $0.08 \times 10^{-3} \mu\text{m}^2$ ). In terms of the characteristics of the Chang 8 Member reservoir, this pore-throat type is moderately exploitable.

- (3) 'Fine nanothroats' are characterized by type-III mercury intrusion curves (Fig. 5(c)) in which the capillary pressure curve increases steadily to only 20%–60% maximum mercury saturation above ~10 MPa. Displacement pressures for this pore-throat type are the highest of the three, averaging 8.93 MPa, and the median pressure is 26.44 MPa on average. The maximum pore throat radius is 0.09  $\mu\text{m}$  on average, the mean radius ranges from 0.02 to 0.04  $\mu\text{m}$  (average 0.03  $\mu\text{m}$ ), and the median radius is 0.03  $\mu\text{m}$  on average. The average sorting coefficient is 0.02. The overall porosity ranges from 0.99% to 6.66% (average 4.48%) with permeabilities of  $0.01\text{--}0.08 \times 10^{-3} \mu\text{m}^2$  (average  $0.04 \times 10^{-3} \mu\text{m}^2$ ). In terms of the Chang 8 Member reservoir, this pore-throat type is poorly exploitable.

#### 4.4. Reservoir classification and evaluation

To classify the reservoir quantitatively, objectively, and accurately, we selected 69 samples from 10 typical wells to form a sample set based on a comprehensive consideration of core descriptions, oil contents, and selected characteristic parameters: porosity, permeability, median pore-throat radius, maximum pore-throat radius, median pressure, pore discharge pressure, chlorite content, and kaolinite content. We performed cluster analysis using SPSS software to form a cluster spectrum diagram (Fig. 6) classifying the Chang 8 Member reservoir into three types based on the values of the characteristic parameters for each type. To validate our reservoir classifications, we compare with actual oil production rates obtained from Sinopec North China Oil and Gas Company.

Type-I reservoirs have the best conditions for hosting tight oil reserves, showing an average trial oil production rate of  $8.85 \text{ m}^3/\text{d}$ . They have the highest porosities (average 12%) and permeabilities (average  $0.2 \times 10^{-3} \mu\text{m}^2$ ), the widest median pore-throat radii (average 0.12  $\mu\text{m}$ ) and maximum pore-throat radii (average 0.88  $\mu\text{m}$ ), and the lowest median capillary pressures (average 10.61 MPa) and pore discharge pressures (average 1.17 MPa). This reservoir type is characterized by the lowest kaolinite contents (average 1.0%) and the highest chlorite contents (average 5.9%).

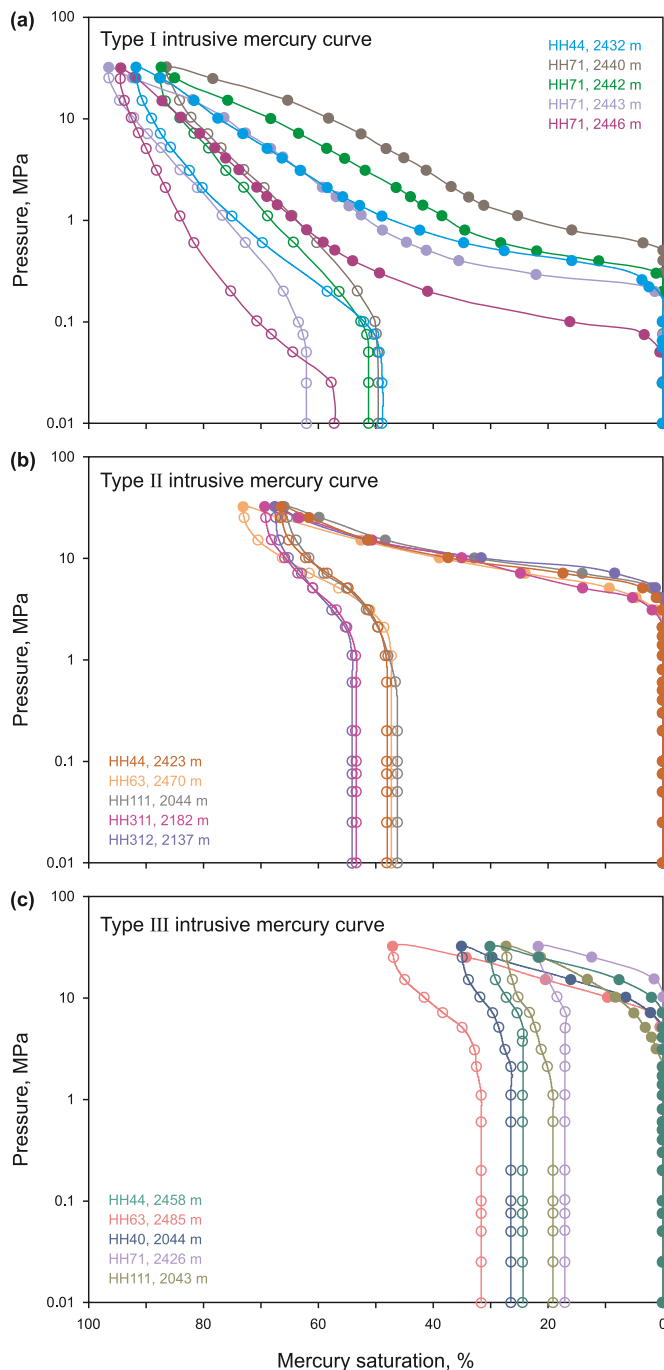


**Fig. 5.** Capillary pressure curves in the Chang 8 Member in the Zhenjing area.

Type-II reservoirs have moderate conditions for hosting tight oil reserves, showing an average trial oil production rate of  $2.64 \text{ m}^3/\text{d}$ . They have moderate porosities (average 10%), permeabilities (average  $0.1 \times 10^{-3} \mu\text{m}^2$ ), median pore-throat radii (average 0.06  $\mu\text{m}$ ), maximum pore-throat radii (average 0.44  $\mu\text{m}$ ), median capillary pressures (average 15.57 MPa), and pore discharge pressures (average 2.42 MPa). This reservoir type is characterized by moderate kaolinite (average 1.0%) and chlorite contents (average 3.5%).

Type-III reservoirs have the worst conditions for hosting tight oil reserves, showing an average trial oil production rate of  $0.48 \text{ m}^3/\text{d}$ . They have the lowest porosities (average 5.0%) and permeabilities

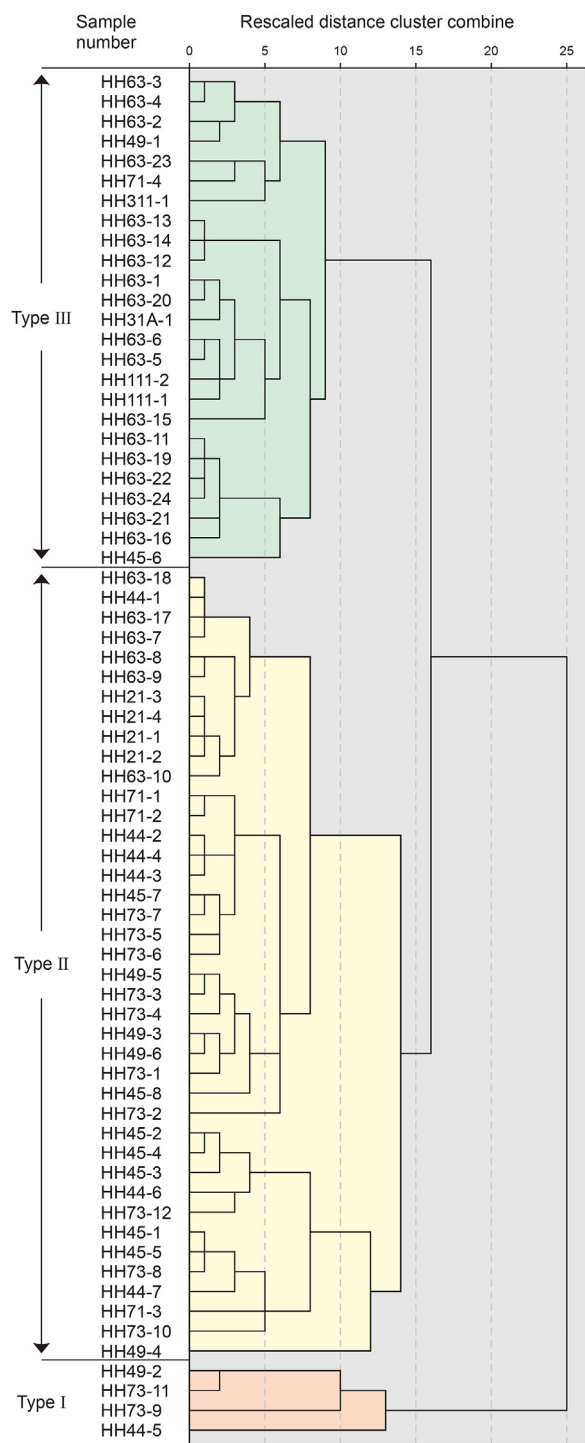


Fig. 6. Pedigree diagram of our reservoir-type cluster analysis of the Chang 8 Member.

(average  $0.05 \times 10^{-3} \mu\text{m}^2$ ), the narrowest median pore-throat radii (average  $0.04 \mu\text{m}$ ) and maximum pore-throat radii (average  $0.15 \mu\text{m}$ ), and the highest median capillary pressures (average 20.53 MPa) and pore discharge pressures (average 5.61 MPa). This reservoir type is characterized by the highest kaolinite contents (average 1.8%) and the lowest chlorite contents (average 1.0%).

#### 4.5. Factors controlling reservoir characteristics

##### 4.5.1. Reservoir characterization based on sedimentary microfacies

Particles in the Chang 8 Member reservoir sandstone are mainly in point to line contacts and permeability is extremely low, classifying this reservoir as an extremely low permeability sandstone reservoir. The formation of this tight sandstone reservoir was mainly controlled by sedimentary characteristics during deposition and subsequent diagenesis. In the study area, this sandstone is mainly a braided-fluvial river delta-front subfacies, and can be further divided into subaqueous distributary channel, interdistributary bay, river-mouth bar, and sheet sand microfacies (Zhang et al., 2012; Wang et al., 2021).

Wang et al. (2021) analyzed microfacies and indicators of the Chang 8 tight reservoirs in the study area. They found that: the subaqueous distributary channel comprises normally graded medium-to fine-grained sandstones marked by a distinctive box- or bell-shaped gamma ray (GR) curve in core logs; the river-mouth bar deposits comprise fine-grained sandstones, often inversely graded, with funnel-shaped GR curves; the sheet sand mainly comprises thin-bedded siltstones with a sharp tooth- or finger-shaped GR curve; and the interdistributary bay mainly comprises mudstone and muddy siltstone. Using their descriptions as a guide, we identified the subaqueous distributary channel, river-mouth bar, and interdistributary bay microfacies in well HHX1 (Fig. 7).

Comparison of these sedimentary microfacies with porosity, permeability, and oil saturation in the Chang 8 Member reservoir in well HHX1 (Fig. 7) indicates that these parameters are generally highest in the subaqueous distributary channel microfacies, moderate in the river-mouth bar microfacies, and lowest in the interdistributary bay microfacies (Fig. 8). This result demonstrates the significant control of sedimentary microfacies type on reservoir physical properties and oil saturation; high-quality reservoirs seem to have formed in the subaqueous distributary channel, consistent with previous results (Lin et al., 2017; Wang et al., 2017; Zhang et al., 2022). Furthermore, porosity, permeability, and oil saturation tend to be higher in the middle–lower parts of the subaqueous distributary channel microfacies and the upper parts of the river-mouth bar microfacies (Fig. 7). Specifically, porosity, permeability, and oil saturation increase towards the top of the river-mouth bar microfacies, then decrease upwards in the subaqueous distributary channel microfacies. This characteristic variation among the sedimentary microfacies indicates a moderate hydrodynamic control on the development of high-quality reservoirs (Liu et al., 2018; Zhang et al., 2022).

Our classification of the Chang 8 Member reservoirs into three types based on multiple parameters improves upon previous research by overcoming the limitations of subjective single-parameter analyses. Based on the correspondence between different reservoir types and their depositional microfacies, we classify the reservoirs as follows. Type-I reservoirs mainly formed as subaqueous distributary channels in high-energy environments characterized by high sedimentation rates and good sorting; they exhibit high porosity (average 12%) and permeability (average  $0.2 \times 10^{-3} \mu\text{m}^2$ ), with trial oil production rates exceeding  $5 \text{ m}^3/\text{d}$ . Type-II reservoirs mainly formed in the moderate-energy environments of river-mouth bars and have finer grain sizes and moderate sorting; they exhibit moderate porosity (average 10%) and permeability ( $0.1 \times 10^{-3} \mu\text{m}^2$ ), with trial oil production rates of  $1\text{--}5 \text{ m}^3/\text{d}$ . Type-III reservoirs mainly formed in the low-energy environments of interdistributary bays and are characterized by fine grain sizes and poor sorting; they exhibit low porosity (average 5%) and permeability ( $0.05 \times 10^{-3} \mu\text{m}^2$ ), with trial oil production rates  $<1 \text{ m}^3/\text{d}$ .

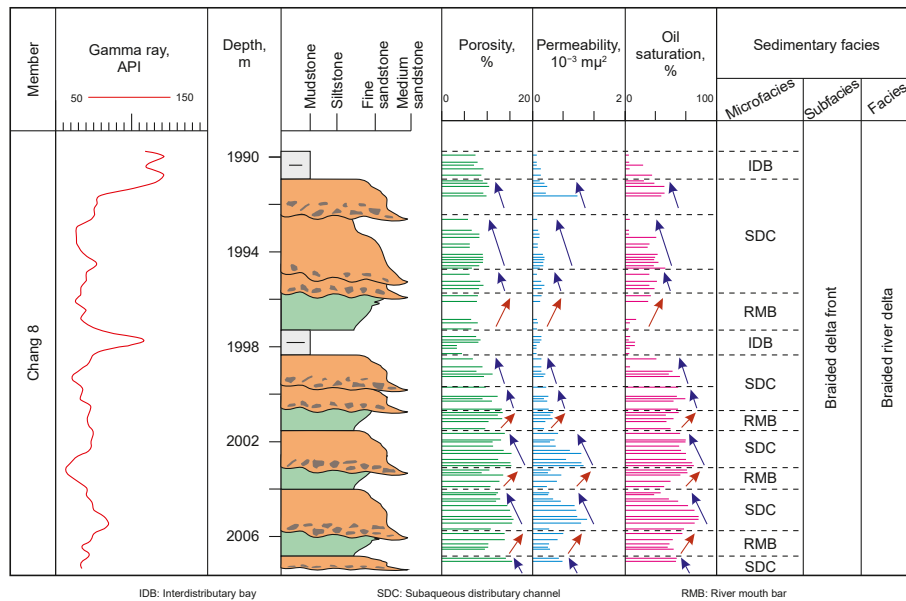


Fig. 7. Stratigraphic correlation of sedimentary microfacies with porosity, permeability, and oil saturation in well HHX1 in the Zhenjing area. Red and blue arrows indicate upward-increasing and upward-decreasing trends, respectively.

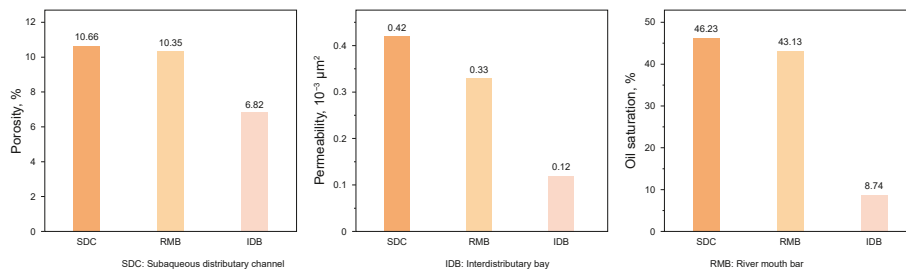


Fig. 8. Porosity, permeability, and oil saturation histograms grouped by sedimentary microfacies for well HHX1.

#### 4.5.2. The diagenetic influence on the reservoir

Previous studies have shown that compaction and cementation are the main diagenetic causes of porosity reduction after sediment deposition (Nguyen et al., 2014; Makeen et al., 2016; Liang and Guo, 2017; Tan et al., 2017; Qian et al., 2019; Ma et al., 2020). Compaction reduced porosity by 57% on average, and cementation reduced porosity by 33% (Fig. 9). In general, compaction is the main control of reservoir density and the main diagenetic process leading to porosity reduction, whereas cementation exerts only a secondary control. Although dissolution is common in Chang 8 Member sandstones, kaolinite (the product of dissolution) fills pores and plugs pore throats. Therefore, dissolution has only a limited effect on this sandstone reservoir.

Fine-grained sandstones are often sensitive to compaction due to the large amount of plastic debris they contain (Shou et al., 2005). Due to its heterogeneous structure, debris tends to have low compressive and thermal resistance, and is thus more prone to deformation under external geological stresses (Milliken, 2001; Shou et al., 2005; Dutton and Loucks, 2010). Plastic debris thus tends to deform under mechanical compaction by overlying strata, plugging pores and pore throats, and resulting in additional deterioration of sandstone reservoir properties beyond that resulting from compaction alone. The Chang 8 Member reservoir contains variable amounts of plastic debris; samples containing less plastic debris are more porous (Fig. 3(f)) than those containing abundant plastic debris (Fig. 3(g)). Indeed, the abundance of plastic debris in

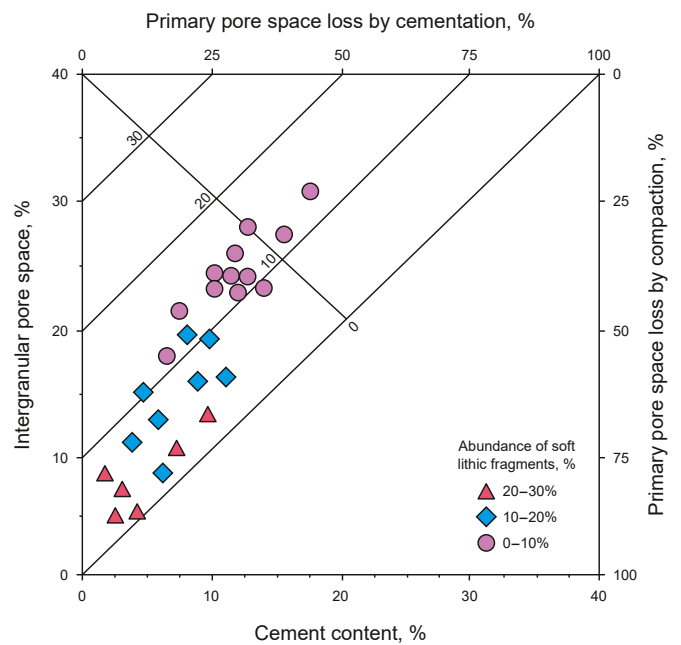


Fig. 9. The effects of compaction and cementation on porosity reduction in the Chang 8 Member in the Zhenjing area.

Chang 8 Member sandstones is positively correlated with the degree of pore reduction (Fig. 9), intensifying the decrease in intergranular volume during diagenesis.

Sandstone grain size also has a certain influence on compaction; smaller grains can more easily slide and rearrange under the load of overlying strata (Milliken, 2001). The main bodies of the subaqueous distributary channel and river-mouth bar microfacies are mainly composed of fine sandstone, but siltstone and pelitic siltstone are often developed along their edges, which may locally lead to more intense compaction.

Calcite cement is common in pores of the Chang 8 Member reservoir, occurring in abundances of 1%–28% (average 5.1%). Calcite content in the Chang 8 Member is weakly negatively correlated with porosity and permeability below about 5% calcite, although porosity and permeability decrease rapidly up to 5% calcite (Fig. 10(a) and (b)). Calcite contents greater than 5% are more strongly negatively correlated with porosity and permeability, but the slope is shallower (Fig. 10(a) and (b)). This phenomenon indicates that 5% calcite content may be a threshold, below which the correlations between calcite content and porosity and permeability

are relatively weak, indicating that calcite cementation is not the main factor causing the deterioration of reservoir physical properties; the rapid decrease of both porosity and permeability at these low calcite contents may be related to the significant negative impact of compaction on reservoir physical properties. At calcite contents >5%, the correlations between calcite content and porosity and permeability are enhanced, which may reflect increased occupation of pore space and plugging of pore throats by calcite cementation; this more drastic reduction of primary pore space makes calcite cementation the main factor negatively affecting reservoir physical properties at higher calcite contents.

Authigenic clay minerals in the Chang 8 Member reservoir within the study area are dominated by kaolinite and chlorite, with less illite (Wang et al., 2018). Previous studies have shown that cladding by chlorite particles can inhibit quartz edge growth and thus protect reservoirs to a certain extent (Bloch et al., 2002; Aminul, 2009). In the Chang 8 Member reservoir, chlorite mainly occurs as cladding particles (Fig. 3(h)–(j)), and our correlation analysis shows that the porosity and permeability of the Chang 8 Member sandstone increase with increasing chlorite content

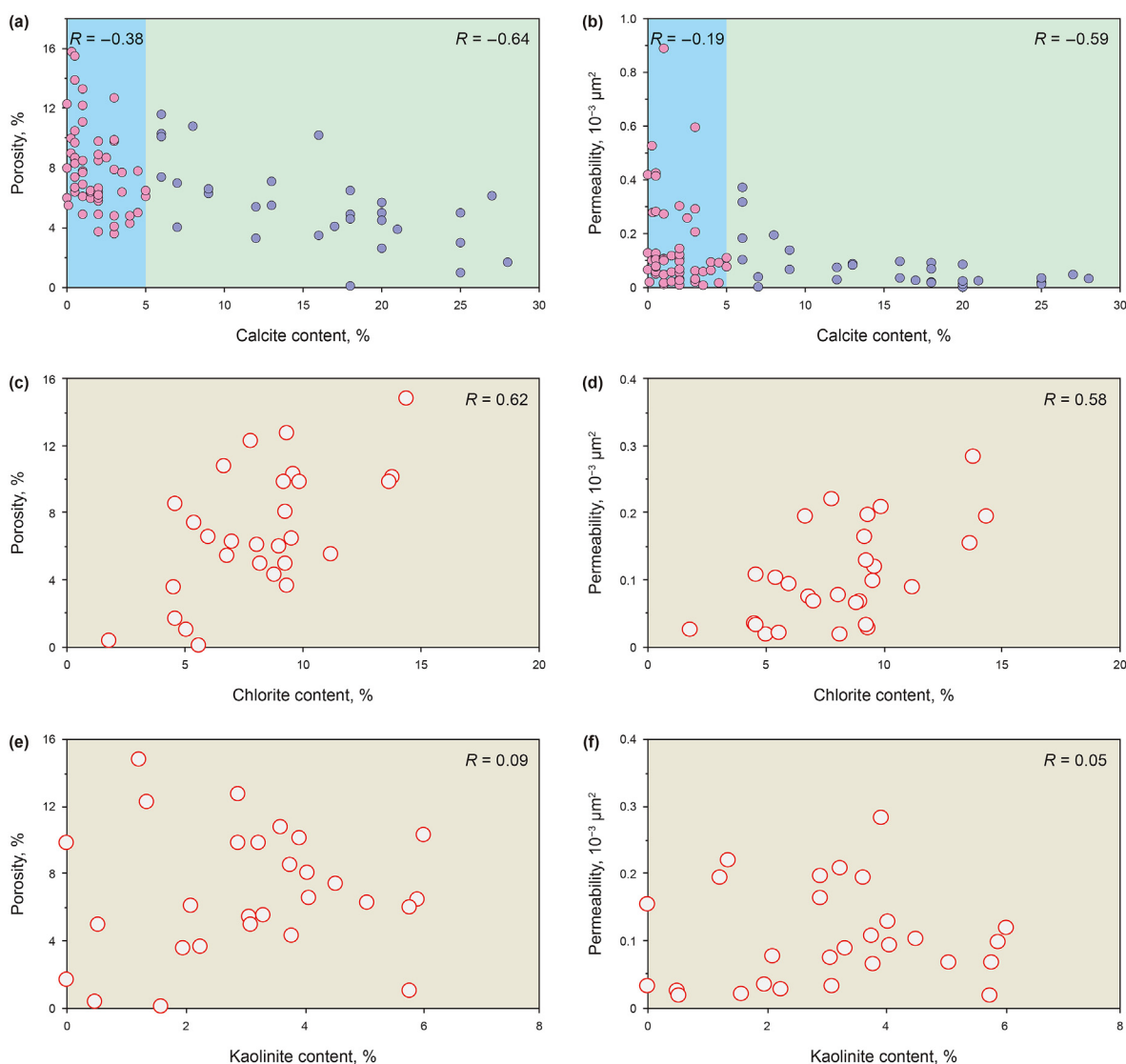


Fig. 10. ((a), (b)) Calcite, ((c), (d)) chlorite, and ((e), (f)) kaolinite contents versus ((a), (c), (e)) porosity and ((b), (d), (f)) permeability in the Chang 8 Member reservoir.

(Fig. 10(c) and (d)). This indicates that chlorite cladding indeed inhibits quartz edge growth in the Chang 8 Member sandstone, limiting the influence of compaction and thereby the degree of quartz cementation as matted crystals in pores, effectively protecting the reservoir. Although it remains controversial whether authigenic chlorite cladding in clastic rocks promotes pore development (Grigsby, 2001; Worden et al., 2006; Zhou et al., 2016; Zhao et al., 2021), our results for the Chang 8 Member support this relationship.

Kaolinite in the Chang 8 Member sandstone mainly occurs as interstitial material in pores (Fig. 3(h)–(k), (l), (n)). Indeed, kaolinite is mainly the product of feldspar dissolution (e.g., Liu et al., 2020); feldspar fills a significant fraction of early primitive intergranular pores, and its dissolution creates secondary pores that are then filled by kaolinite precipitation. Therefore, the pores generated by feldspar dissolution are roughly equivalent to the space occupied by kaolinite precipitation and accumulation (Fig. 3(k), (l), (n)). Accordingly, this self-replacing process of feldspar dissolution and kaolinite precipitation in the Chang 8 Member sandstone has only limited influence on porosity, consistent with the low correlation coefficients between kaolinite and porosity and permeability in our correlation analysis (Fig. 10(e) and (f)).

Our quantitative evaluation of this reservoir demonstrates that porosity, permeability, median and maximum pore-throat radii, and chlorite content decrease from type-I to type-III reservoirs, whereas the median capillary pressure, pore discharge pressure, and kaolinite content increase. These results highlight that the quality of the Chang 8 Member reservoir varies greatly between layers. Chlorite cladding significantly inhibits reservoir densification, whereas kaolinite fills pore spaces and promotes densification. These results are consistent with previous analyses, indicating that

using cluster analysis to quantitatively classify reservoirs is feasible and can be used to better evaluate the Chang 8 Member reservoir.

#### 4.5.3. Diagenetic sequence

Based on our results, the diagenetic sequence of the Chang 8 Member tight sandstone reservoirs is as follows (Fig. 11). Initially, the reservoirs underwent early mechanical compaction that reduced pore spaces between grains. This was followed by the formation of chlorite film, early carbonate cementation, and early siliceous cementation, which further reduced porosity. Subsequently, feldspar dissolution created secondary porosity. Over time, hydrocarbon filling proceeded, and the reservoirs underwent late siliceous cementation and carbonate cementation, which further diminished the pore space and ultimately affected the reservoir's physical properties.

From the sedimentation of the Chang 8 Member until the late Middle Jurassic, as the basin continued to subside, the quick compaction of the sediments gradually deteriorated the reservoir's physical properties; the porosities of highly heterogeneous sandstones rapidly decreased to form dense sandstones. From the late Middle Jurassic to the middle Late Cretaceous, the Chang 8 Member reservoirs underwent continued slow compaction and significant diagenesis, characterized by alternating dissolution and rapid cementation that further reduced porosity and deteriorated reservoir physical properties. Since the middle Late Cretaceous, continued diagenesis of the Chang 8 Member reservoirs was characterized by alternating dissolution and cementation processes. This stage of complex and diverse diagenesis further evolved the reservoir's pore structure and porosity (Fig. 11).

Diagenetic evolution and pore evolution analyses were carried out for the subaqueous distributary channel, river-mouth bar, and

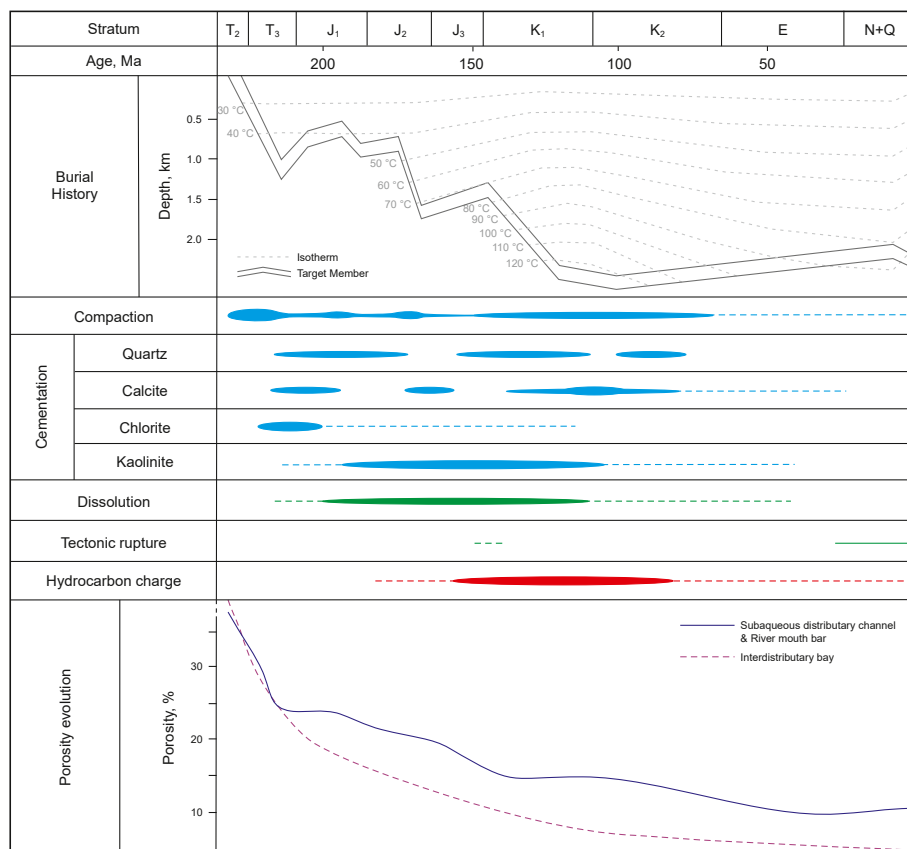


Fig. 11. Summary diagram of diagenesis and the evolution of the porosity of tight sandstone reservoirs in the Chang 8 Member in the study area.

interdistributary bay. In general, the interdistributary bay is dominated by muddy sedimentation, and the pore space is gradually compacted and densified with the increase of the burial depth (Fig. 11). However, the pore evolution of the subaqueous distributary channel and river-mouth bar has similarity, and the compacting effect resulted in fewer pore spaces in the early stage with the increase of the burial depth (Fig. 11). The oil filling led to the partial dissolution of feldspar, which also inhibited the pore space from being filled by cementation, slowed down the reduction of pore space, and favored the preservation of pore space so far. Tectonic uplift and rupture during the Himalayan period may had a positive effect on the reservoir (e.g., Dang et al., 2018; Guo et al., 2019).

Throughout its diagenesis, the densification process and mechanism of the reservoir have been primarily influenced by rock constituent as well as cementation. The high content of plastic rock debris in the rock can lead to rapid compaction and accelerate the densification process of the rock (e.g., Liu et al., 2020), while carbonate cementation, siliceous cementation, and kaolinite cementation also plays an important role in reservoir densification. The combined effects of these processes have significantly altered the physical properties and fluid transmission capabilities of the Chang 8 Member tight sandstone reservoirs.

#### 4.6. Reservoir densification mechanism

Reservoir densification is important to the formation and preservation of tight sandstone reservoirs, and even hydrocarbon charging (Liang and Guo, 2017; Liu et al., 2020; Ma et al., 2020; Shi et al., 2021). Therefore, based on our analysis of the reservoir

characteristics and main factors controlling reservoir quality, we propose three reservoir densification mechanisms for the Chang 8 Member in the Zhenjing area: the persistent densification of highly plastic rock debris, calcite cementation, and feldspar dissolution/kaolinite precipitation and siliceous cementation (Fig. 12).

- (1) Densification of plastic rocks during burial. The persistent densification of highly plastic rocks (Fig. 12(a)) occurs in sandstones containing abundant plastic rock debris and mud (Fig. 3(g)). The rock debris and mud plastically deform during burial, leading to rapid dehydration and compaction, and thus the rapid densification of the reservoir. However, if the remaining pores are not connected by fractures at a later stage, continued densification can prevent the release of pore space by subsequent dissolution.
- (2) Densification via calcite cementation. Calcite cementation (Fig. 12(b)) usually occurs in rocks with less interstitial material. Calcite cement forms contemporaneously with strong evaporation and exposure to water during shallow burial (Fig. 3(c) and (d)). Because chlorite clads the surrounding grains, it must have formed earlier than the calcite cement (Fig. 3(o)). This type of early densification can later release a certain amount of reservoir space due to rupturing and fluid dissolution.
- (3) Densification via kaolinite precipitation and siliceous cementation. Feldspar dissolution and subsequent kaolinite precipitation and siliceous cementation (Fig. 12(c)) occurs in feldspar-rich rocks (Fig. 3(l)). During burial, feldspar dissolves to form kaolinite, opening secondary intragranular dissolved pores that are then filled by kaolinite and siliceous

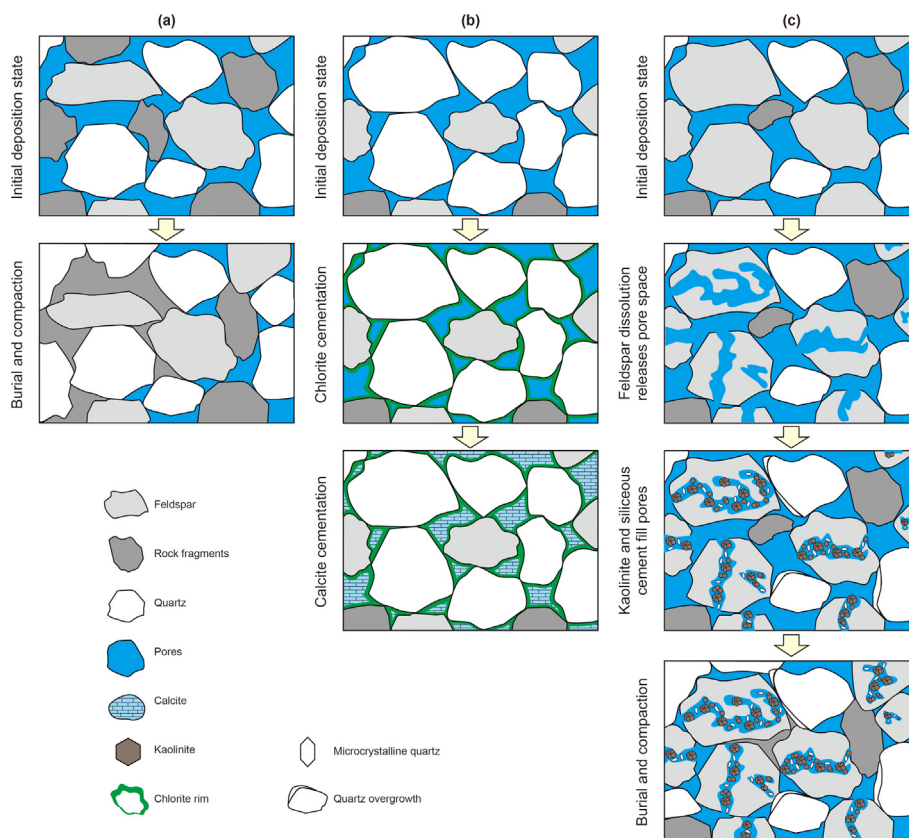


**Fig. 12.** Schematic diagrams of the three densification mechanisms operating in the Chang 8 Member reservoir in the Zhenjing area: (a) the persistent densification of highly plastic rock debris during burial and compaction; (b) chlorite cementation and subsequent calcite cementation and pore filling; and (c) feldspar dissolution and subsequent kaolinite precipitation and siliceous cementation, which effectively fills the pores remaining after feldspar dissolution.

cement. Upon further burial, the pore space released by feldspar and kaolinite is further compacted and densified.

The persistent densification of highly plastic rock debris is the most common densification mechanism in the Chang 8 Member in the study area. Fig. 3(f)–(i), and (j) show that hydrocarbon charging generally occurs later than reservoir densification. This result, combined with the results of our microfacies analysis (Figs. 7 and 8) and comprehensive reservoir analysis, indicate that the middle and lower parts of subaqueous distributary channel microfacies in the lower part of the Chang 8 Member represent the highest quality reservoirs in the study area.

## 5. Conclusions

We combined comprehensive descriptions of rocks from the Chang 8 Member sandstone reservoir in the Zhenjing area with previous results to systematically characterize the reservoir rocks. The Chang 8 Member reservoir is an extremely low permeability tight sandstone reservoir of low maturity, and the rocks are mainly composed of lithic feldspar sandstone and subordinate feldspar lithic sandstone. Pore space in the reservoir is mainly characterized by intergranular dissolved pores, intragranular dissolved pores, residual primary intergranular pores, intergranular micropores, and a small proportion of micro-fractures. Pore-throats are narrow; the largest and most permeable are microthroats, and throat sizes decrease to less-permeable coarse and fine nanthroats.

The development of high-quality reservoirs in the Chang 8 Member in the study area is mainly controlled by sedimentary microfacies and the abundances of plastic rock debris, carbonate, and clay minerals. The middle and lower parts of subaqueous distributary channel microfacies are the most favorable for reservoir development. The abundance of plastic debris is positively correlated with the reduction of pore space. Calcite cementation negatively affects reservoir physical properties when the calcite content is greater than 5%. Kaolinite precipitation replacing feldspar dissolution has both constructive and destructive effects on the Chang 8 Member reservoir, whereas chlorite cladding of particles acts to support the reservoir.

We used a comprehensive cluster analysis of eight reservoir parameters (porosity, permeability, median pore-throat radius, maximum pore-throat radius, median capillary pressure, pore discharge pressure, chlorite content, and kaolinite content) to classify the Chang 8 reservoir in the study area into three types. Type-I reservoirs are the most porous and permeable, have the widest pore-throat radii, the smallest median capillary pressures and pore discharge pressures, the highest chlorite contents, and the lowest kaolinite contents. Trial oil production rates from these reservoirs exceed 5 m<sup>3</sup>/d. They are generally found in subaqueous distributary channels, representing the best quality reservoirs and thus the most favorable exploration targets in the Chang 8 Member in the study area.

We suggest that the persistent densification of highly plastic rock debris, calcite cementation, and feldspar dissolution followed by subsequent kaolinite precipitation and siliceous cementation are the main mechanisms of reservoir densification for the Chang 8 Member.

## CRediT authorship contribution statement

**Yi-Quan Ma:** Writing – review & editing, Writing – original draft, Visualization, Methodology, Investigation, Data curation, Conceptualization. **Chen Zhang:** Writing – review & editing, Methodology, Data curation, Conceptualization. **Yong-Chao Lu:** Writing – review & editing, Resources, Investigation,

Conceptualization. **Xiang-Ye Kong:** Writing – review & editing, Methodology. **Ying Guo:** Writing – review & editing, Visualization, Methodology, Data curation. **Yi-Xin Dong:** Writing – review & editing. **Lin Chen:** Writing – review & editing, Methodology, Investigation. **Rong Qi:** Writing – review & editing, Resources, Investigation. **Feng-Cun Xing:** Writing – review & editing, Methodology, Investigation, Data curation.

## Declaration of competing interest

The authors declare that they have no known competing financial interests or personal relationships that could have appeared to influence the work reported in this paper.

## Acknowledgements

We thank the Research Institute of Petroleum Exploration and Development of Sinopec North China Oil and Gas Company for providing geological data and their laboratory assistances. We also thank the five anonymous reviewers for their valuable and constructive comments and suggestions. This work was supported by Natural Science Foundation of Sichuan Province (2022NSFSC1075) and National Natural Science Foundation of China (42072137).

## References

- Ameen, M.S., MacPherson, K., Al-Marhoon, M.I., Rahim, Z., 2012. Diverse fracture properties and their impact on performance in conventional and tight-gas reservoirs, Saudi Arabia: the Unayzah, South Haradh case study. AAPG (Am. Assoc. Pet. Geol.) Bull. 96, 459–492. <https://doi.org/10.1306/06011110148>.
- Aminul, I.M., 2009. Diagenesis and reservoir quality of bhuvan sandstones (neogene), titas gas field, bengal basin, Bangladesh. J. Asian Earth Sci. 35, 89–100. <https://doi.org/10.1016/j.jseaes.2009.01.006>.
- Bloch, S., Lander, R.H., Bonnell, L., 2002. Anomalously high porosity and permeability in deeply buried sandstone reservoirs: origin and predictability. AAPG (Am. Assoc. Pet. Geol.) Bull. 86, 301–328. <https://doi.org/10.1306/61EEDABC-173E-11D7-8645000102C1865D>.
- Chen, L., Lu, Y., Wu, J., Xing, F., Liu, L., Ma, Y., Rao, D., Peng, L., 2015. Sedimentary facies and depositional model of shallow water delta dominated by fluvial for Chang 8 oil-bearing group of Yanchang Formation in southwestern Ordos Basin, China. J. Cent. South. Univ. 22, 4749–4763. <https://doi.org/10.1007/s11771-015-3027-3>.
- Cui, X., Radwan, A., 2022. Coupling relationship between current in-situ stress and natural fractures of continental tight sandstone oil reservoirs. Interpretation 10, SF9–SF21. <https://doi.org/10.1190/INT-2021-0200.1>.
- Dang, B., Zhao, H., Qu, M., Wang, T., Mi, W., Guo, X., Fan, J., Liu, P., 2018. Distribution characteristics, genesis analyses, and research significance of Triassic regional structural fractures in the Ordos Basin, Central China. Geol. J. 53, 212–224. <https://doi.org/10.1002/gj.3165>.
- Debenham, N., Farrell, N., Holford, S., King, R., Healy, D., 2019. Spatial distribution of micrometre-scale porosity and permeability across the damage zone of a reverse-reactivated normal fault in a tight sandstone: insights from the Otway Basin, SE Australia. Basin Res. 31, 640–658. <https://doi.org/10.1111/bre.12345>.
- Deng, S., Lu, Y., Luo, Z., Fan, R., Li, X., Zhao, Y., Ma, X., Zhu, R., Cui, J., 2018. Subdivision and age of the Yanchang Formation and the middle/upper triassic boundary in Ordos Basin, north China. Sci. China Earth Sci. 61, 1419–1439. <https://doi.org/10.1007/s11430-017-9215-3>.
- Ding, X., Zhang, S., Xie, S., Yi, C., 2011. Main controlling factors analysis of low permeable tight reservoirs of Chang 8 formation in Zhenjing area. J. Southwest Petrol. Univ. (Sci. Technol. Edition) 33, 25–30. <https://doi.org/10.3863/j.issn.1674-5086.2011.01.005> (in Chinese).
- Dou, W., Liu, L., Wu, K., Xu, Z., Feng, X., 2017. Origin and significance of secondary porosity: a case study of upper Triassic tight sandstones of Yanchang Formation in Ordos Basin, China. J. Petrol. Sci. Eng. 149, 485–496. <https://doi.org/10.1016/j.petrol.2016.10.057>.
- Duan, Y., Wang, C., Zheng, C., Wu, B., Zheng, G., 2008. Geochemical study of crude oils from the Xifeng oilfield of the Ordos Basin, China. J. Asian Earth Sci. 31, 341–356. <https://doi.org/10.1016/j.jseaes.2007.05.003>.
- Dutton, S., Loucks, R., 2010. Diagenetic controls on evolution of porosity and permeability in lower Tertiary Wilcox sandstones from shallow to ultradeep (200–6700 m) burial, Gulf of Mexico Basin. U.S.A. Mar. Petrol. Geol. 27, 69–81. <https://doi.org/10.1016/j.marpetgeo.2009.08.008>.
- Folk, R.L., Andrews, P.B., Lewis, D.W., 1970. Detrital sedimentary rock classification and nomenclature for use in New Zealand. N. Z. J. Geol. Geophys. 13, 937–968. <https://doi.org/10.1080/00288306.1970.10418211>.

- Fu, D., Xu, J., Wang, G., 2011. Reservoir classification and evaluation based on Q cluster analysis combined with Bayesian discrimination algorithm. *Sci. Technol. Rev.* 29, 29–33. <https://doi.org/10.3981/j.issn.1000-7857.2011.03.003> (in Chinese).
- Gao, M., Xu, S., Zhuo, H., Wang, Y., Wu, S., 2020. Coupling relationship between shelf-edge trajectories and slope morphology and its implications for deep-water oil and gas exploration: a case study from the passive continental margin, East Africa. *J. Earth Sci.* 31, 820–833. <https://doi.org/10.1007/s12583-020-1288-8>.
- Grigsby, J.D., 2001. Origin and growth mechanism of authigenic chlorite in sandstones of the lower Vicksburg Formation, south Texas. *J. Sediment. Res.* 71, 27–36. <https://doi.org/10.1306/060100710027>.
- Guo, P., Ren, D., Xue, Y., 2019. Simulation of multi-period tectonic stress fields and distribution prediction of tectonic fractures in tight gas reservoirs: a case study of the Tianhuan Depression in western Ordos Basin, China. *Mar. Petrol. Geol.* 109, 530–546. <https://doi.org/10.1016/j.marpetgeo.2019.06.026>.
- Hao, L., Tang, J., Wang, Q., Tao, H., Ma, X., Ma, D., Ji, H., 2017. Fractal characteristics of tight sandstone reservoirs: a case from the upper triassic Yanchang Formation, Ordos Basin, China. *J. Petrol. Sci. Eng.* 158, 243–252. <https://doi.org/10.1016/j.petrol.2017.08.060>.
- Ji, L.M., Yan, K., Meng, F.W., Zhao, M., 2010. The oleaginous *botryococcus* from the triassic Yanchang Formation in Ordos Basin, northwestern China: morphology and its paleoenvironmental significance. *J. Asian Earth Sci.* 38, 175–185. <https://doi.org/10.1016/j.jseaeas.2009.12.010>.
- Jia, C., Zheng, M., Zhang, Y., 2012. Unconventional hydro-carbon resources in China and the prospect of exploration and development. *Petrol. Explor. Dev.* 39, 129–136. [https://doi.org/10.1016/S1876-3804\(12\)60026-3](https://doi.org/10.1016/S1876-3804(12)60026-3).
- Jia, J., Sima, L., Meng, J., Meng, Y., 2016. Comprehensive evaluation of effectiveness of dual-porosity sandstone reservoir: a case study from Chang 81 reservoir in Honghe oilfield in southwest of the Ordos Basin. *Oil Gas Geol.* 37, 238–244. <https://doi.org/10.11743/ogg20160212> (in Chinese).
- Jin, X., Baranyi, V., Caggiati, M., Franceschi, M., Wall, C.J., Liu, G., Schmitz, M., Gianolla, P., Ogg, J., Lu, G., Lu, G., Preto, N., 2021. Middle Triassic lake deepening in the Ordos Basin of North China linked with global sea-level rise. *Global Planet. Change* 207, 103670. <https://doi.org/10.1016/j.gloplacha.2021.103670>.
- Lai, J., Wang, G., Wang, Z., Chen, J., Pang, X., Wang, S., Zhou, Z., He, Z., Qin, Z., Fan, X., 2018. A review on pore structure characterization in tight sandstones. *Earth Sci. Rev.* 177, 436–457. <https://doi.org/10.1016/j.earscirev.2017.12.003>.
- Li, J., Yang, Z., Wu, S., Pan, S., 2021. Key issues and development direction of petroleum geology research on source rock strata in China. *Adv. Geo-Energy Res.* 5, 121–126. <https://doi.org/10.46690/ager.2021.02.02>.
- Li, N., Liu, L., Zheng, R., Lu, D., Zhu, Y., Sun, Y., 2011. Super-low permeability reservoir evaluation in Zhenjing area, Ordos Basin. *Lit. Res.* 23, 41–45. <https://doi.org/10.3969/j.issn.1673-8926.2011.02.008> (in Chinese).
- Li, Y., Tang, D., Xu, H., Yu, T., 2014. In-situ stress distribution and its implication on coalbed methane development in Liulin area, eastern Ordos Basin, China. *J. Petrol. Sci. Eng.* 122, 488–496. <https://doi.org/10.1016/j.petrol.2014.08.010>.
- Liang, C., Guo, J., 2017. Diagenesis and reservoir characteristics of tight sandstones of Chang 81 member of Yanchang Formation in Honghe oilfield. *Ordos Basin. Petrol. Geol. Recov. Effic.* 24, 57–63. <https://doi.org/10.13673/j.cnki.cn37-1359/te.2017.01.008> (in Chinese).
- Lin, W., Chen, L., Lu, Y., Hu, H., Liu, L., 2017. Tight reservoir evaluation of the Chang 8 oil group in the Zhenjing area, southwestern Ordos Basin. *Geol. Explor.* 53, 381–389. <https://doi.org/10.13712/j.cnki.dzykt.2017.02.019> (in Chinese).
- Liu, G., Ma, S., Zhang, Z., Mao, Z., Han, T., Shi, Z., 2023. U–Pb ages of tuff from the Triassic Yanchang Formation in the Ordos Basin: constraints on palaeoclimate and tectonics. *Mar. Petrol. Geol.* 150, 106128. <https://doi.org/10.1016/j.marpetgeo.2023.106128>.
- Liu, H., Yang, Y., Wang, F., Deng, X., Liu, Y., Nan, J., Wang, J., Zhang, H., 2018. Micro-pore and throat characteristics and origin of tight sandstone reservoirs: a case study of the Triassic Chang 6 and Chang 8 members in Longdong area, Ordos Basin, NW China. *Petrol. Explor. Dev.* 45, 223–234. [https://doi.org/10.1016/S1876-3804\(18\)30027-2](https://doi.org/10.1016/S1876-3804(18)30027-2).
- Liu, Y., Xian, C., Li, Z., Wang, J., Ren, F., 2020. A new classification system of lithic-rich tight sandstone and its application to diagnosis high-quality reservoirs. *Adv. Geo-Energy Res.* 4, 286–295. <https://doi.org/10.46690/ager.2020.03.06>.
- Lv, W., Zeng, L., Zhou, S., Ji, Y., Liang, F., Hui, C., Wei, J., 2020. Micro fracture characteristics and its controlling factors in the tight oil sandstones in the southwest Ordos Basin: case study of the eighth member of the Yanchang Formation in Honghe oilfield. *Nat. Gas Geosci.* 31, 37–46. <https://doi.org/10.11764/j.issn.1672-1926.2019.08.006> (in Chinese).
- Ma, L., Qiu, G., Liu, C., Hu, C., Luo, Y., 2020. The relationship between reservoir densification and petroleum accumulation of the Yanchang Formation in the Honghe oilfield, Ordos Basin. *Acta Sedimentol. Sin.* 38, 620–634. <https://doi.org/10.14027/j.issn.1000-0550.2019.086> (in Chinese).
- Makeen, Y.M., Abdullah, W.H., Ayinla, H.A., Hakimi, M.H., Sia, S.G., 2016. Sedimentology, diagenesis and reservoir quality of the upper abu gabra formation sandstones in the Fula sub-basin, muglad basin, Sudan. *Mar. Petrol. Geol.* 77, 1227–1242. <https://doi.org/10.1016/j.marpetgeo.2016.08.015>.
- Milliken, K., 2001. Diagenetic heterogeneity in sandstone at the outcrop scale, Breathitt Formation (Pennsylvanian), eastern Kentucky. *AAPG (Am. Assoc. Pet. Geol.) Bull.* 85, 795–815. <https://doi.org/10.1306/8626CA05-173B-11D7-8645000102C1865D>.
- Nguyen, V.H., Gland, N., Dautriat, J., David, C., Wassermann, J., Guélard, J., 2014. Compaction, permeability evolution and stress path effects in unconsolidated sand and weakly consolidated sandstone. *Int. J. Rock Mech. Min. Sci.* 67, 226–239. <https://doi.org/10.1016/j.ijrmm.2013.07.001>.
- Qian, W., Yin, T., Hou, G., 2019. A new method for clastic reservoir prediction based on numerical simulation of diagenesis: a case study of the Ed1 clastic sandstones in the Bozhong Depression, Bohai Bay Basin, China. *Adv. Geo-Energy Res.* 3, 82–93. <https://doi.org/10.26804/ager.2019.01.07>.
- Qiu, X., Liu, C., Mao, G., Deng, Y., Wang, F., Wang, J., 2014. Late Triassic tuff intervals in the Ordos Basin, Central China: their depositional, petrographic, geochemical characteristics and regional implications. *J. Asian Earth Sci.* 80, 148–160. <https://doi.org/10.1016/j.jseaeas.2013.11.004>.
- Ritts, B.D., Weislogel, A., Graham, S.A., Darby, B.J., 2009. Mesozoic tectonics and sedimentation of the giant polyphase nonmarine intraplate Ordos Basin, western North China block. *Int. Geol. Rev.* 51, 95–115. <https://doi.org/10.1080/00206810802614523>.
- Scotese, C.R., 2014. Atlas of middle & late permian and triassic paleogeographic maps, maps 43–48 from volume 3 of the PALEOMAP atlas for ArcGIS (jurassic and triassic) and maps 49–52 from volume 4 of the PALEOMAP PaleoAtlas for ArcGIS (late paleozoic). In: Mollweide Projection. PALEOMAP Project, Evanston, IL.
- Shi, B., Chang, X., Yin, W., Li, Y., Mao, L., 2019. Quantitative evaluation model for tight sandstone reservoirs based on statistical methods—a case study of the Triassic Chang 8 tight sandstones, Zhenjing area, Ordos Basin, China. *J. Petrol. Sci. Eng.* 173, 601–616. <https://doi.org/10.1016/j.petrol.2018.10.035>.
- Shi, J., Lin, Y., Zhao, A., Wang, X., An, K., Zhong, X., Hu, K., Zhu, Y., Liu, L., 2021. Diagenetic features and porosity dense evolution of Chang 8 tight sandstone reservoir in Huijianshan area, Ordos Basin. *J. Pet. Explor. Prod.* 11, 1037–1051. <https://doi.org/10.1007/s13202-021-01092-7>.
- Shou, J., Zhang, H., Si, C., Wang, X., Chen, Z., Wang, S., 2005. *Dynamic Diagenesis of Sandstone*. Petroleum Industry Press, Beijing, pp. 1–153 (in Chinese).
- Sun, L., Zou, C., Jia, A., Wei, Y., Zhu, R., Wu, S., Guo, Z., 2019. Development characteristics and orientation of tight oil and gas in China. *Petrol. Explor. Dev.* 46, 1073–1087. [https://doi.org/10.1016/S1876-3804\(19\)60264-8](https://doi.org/10.1016/S1876-3804(19)60264-8).
- Tan, Z., Wang, W., Li, W., Lu, S., He, T., 2017. Controlling factors and physical property cutoffs of the tight reservoir in the Liuhe Basin. *Adv. Geo-Energy Res.* 1, 190–202. <https://doi.org/10.26804/ager.2017.03.06>.
- Tang, J., Wang, Q., Ma, X., Liao, P., Hao, L., 2012. Application of Q-type cluster analysis and discriminatory analysis in reservoir evaluation-taking reservoir Chang 81 of Jiyuan area in Ordos Basin as an example. *Special Oil Gas Reservoirs* 19, 28–31. <https://doi.org/10.3969/j.issn.1006-6535.2012.06.006> (in Chinese).
- Wang, F., Yi, W., Chen, C., 2017. Forming mechanisms of reservoir “sweet spots” in tight sandstones of Chang8 Formation, Honghe oil field, Ordos Basin. *Petrol. Geol. Exp.* 39, 484–490. <https://doi.org/10.11781/sydsydz201704484> (in Chinese).
- Wang, M., Xia, D., Wu, Y., Pang, W., Zou, M., 2018. Diagenesis features of Chang 8 tight sandstone reservoir in Honghe oil field, Ordos Basin. *Petrol. Geol. Exp.* 40, 786–792. <https://doi.org/10.11781/sydsydz201806786> (in Chinese).
- Wang, Q., Yang, W., Ge, Y., Song, Y., Jiang, Z., Luo, Q., Zuo, R., Li, Y., Liu, Z., Zhang, F., Wang, Y., Lu, J., 2021. Diagenetic responses to delta front-lacustrine depositional microfacies and implications for tight reservoir quality differences in the Yanchang Formation, western Ordos Basin. *Acta Sedimentol. Sin.* 39, 841–862. <https://doi.org/10.14027/j.issn.1000-0550.2020.112> (in Chinese).
- Worden, R.H., Needham, S.J., Cuadros, J., 2006. The worm gut: a natural clay mineral factory and a possible cause of diagenetic grain coats in sandstones. *J. Geochem. Explor.* 89, 428–431. <https://doi.org/10.1016/j.jexplo.2005.12.011>.
- Xie, R., Zhou, W., Liu, C., Yin, S., Radwan, A., Lei, W., Cai, W., 2022. Experimental investigation on dynamic and static rock mechanical behavior, failure modes, and sequences of frequent interbedded sand and shale reservoirs. *Interpretation* 10, SF23–SF36. <https://doi.org/10.1190/INT-2021-0238.1>.
- Yang, H., Deng, X.Q., 2013. Deposition of Yanchang Formation deep-water sandstone under the control of tectonic events, Ordos Basin. *Petrol. Explor. Dev.* 40, 549–557. [https://doi.org/10.1016/S1876-3804\(13\)60072-5](https://doi.org/10.1016/S1876-3804(13)60072-5).
- Yang, R., Jin, Z., Van Loon, A.J., Han, Z., Fan, A., 2017a. Climatic and tectonic controls of lacustrine hyperpycnite origination in the Late Triassic Ordos Basin, central China: implications for unconventional petroleum development. *AAPG (Am. Assoc. Pet. Geol.) Bull.* 101, 95–117. <https://doi.org/10.1306/06101615095>.
- Yang, Y., Li, W., Ma, L., 2005. Tectonic and stratigraphic controls of hydrocarbon systems in the Ordos Basin: a multicycle cratonic basin in central China. *AAPG (Am. Assoc. Pet. Geol.) Bull.* 89, 255–269. <https://doi.org/10.1306/10070404027>.
- Yang, Z., Zeng, J., Han, F., Feng, X., Feng, S., Zhang, Y., Qiao, J., 2017b. Characterization of microscopic pore texture of Chang 6–Chang 8 members, tight sandstone reservoirs in the southwestern part of Ordos Basin, China. *Nat. Gas Geosci.* 28, 909–919. <https://doi.org/10.11764/j.issn.1672-1926.2017.06.002> (in Chinese).
- Zhang, X., Lin, C., Chen, Z., Pan, F., Zhou, J., Yu, H., 2012. The reservoir characteristics of Chang 8 oil layer group from the Yanchang Formation in Zhenjing area, Ordos Basin. *Geol. J. China Univ.* 18, 328–340. <https://doi.org/10.16108/j.issn1006-7493.2012.02.008> (in Chinese).
- Zhang, X., Liu, Y., Zhang, P., Wang, G., Li, D., Ma, Y., Jiang, C., Bao, M., Chen, K., Liu, B., Xie, Y., 2022. Reservoir classification evaluation and prediction in terms of sedimentary microfacies: a case study from Chang 8 section in Huanxi-Pengyang south section, Ordos Basin. *Acta Sedimentol. Sin.* 40, 534–546. <https://doi.org/10.14027/j.issn.1000-0550.2020.076> (in Chinese).
- Zhao, W.B., Hu, S.Y., Deng, X.Q., Bai, B., Tao, S.Z., Sun, B., Wang, Q.R., Cheng, D.X., 2021. Physical property and hydrocarbon enrichment characteristics of tight oil reservoir in Chang 7 division of Yanchang Formation, Xin’anbian oilfield, Ordos Basin, China. *Petrol. Sci.* 18, 1294–1304. <https://doi.org/10.1016/>

- [j.petsci.2020.07.001](https://doi.org/10.1016/j.petsci.2020.07.001).
- Zhong, X., Liu, L., Wang, H., Xu, Z., Chen, H., Wang, X., Zhu, Y., 2022. Characteristics and origins of the modal pore throat structure in weakly cemented sandy conglomerate reservoirs. *J. Petrol. Sci. Eng.* 208, 109470. <https://doi.org/10.1016/j.petrol.2021.109470>.
- Zhou, Y., Ji, Y., Xu, L., Che, S., Niu, X., Wan, L., Zhou, Y., Li, Z., You, Y., 2016. Controls on reservoir heterogeneity of tight sand oil reservoirs in Upper Triassic Yanchang Formation in Longdong area, southwest Ordos Basin, China: implications for reservoir quality prediction and oil accumulation. *Mar. Petrol. Geol.* 78, 110–135. <https://doi.org/10.1016/j.marpetgeo.2016.09.006>.
- Zou, C.N., Zhang, X.Y., Luo, P., Wang, L., Luo, Z., Liu, L.H., 2010. Shallow-lacustrine sand-rich deltaic depositional cycles and sequence stratigraphy of the upper triassic Yanchang Formation, Ordos Basin, China. *Basin Res.* 22, 108–125. <https://doi.org/10.1111/j.1365-2117.2009.00450.x>.